computer sciences and mathematics forum

MDPI

Proceeding Paper

Stochastic Dynamics of a Harvested Two Species Fishery Model with Random Birth and Death Effects †

Pamodya Teshini Thalawage * and Mihiri Madushani De Silva

Department of Mathematics, Faculty of Science, University of Kelaniya, Kelaniya 11600, Sri Lanka; mihiris@kln.ac.lk

* Correspondence: teshini2000@gmail.com; Tel.: +94-75-881-8866

† Presented at the 2nd International Online Conference on Mathematics and Applications, 10–12 June 2026; Available online: https://sciforum.net/event/IOCMA2026.

Abstract

Bioeconomic management often employs deterministic differential equations which disregard population fluctuations caused by demographic stochasticity. Two Itô stochastic differential equation (SDE) models based on the continuous-time Markov chain (CTMC) model for harvesting two-species systems are presented and compared in this study. The standard aggregate diffusion model is compared against a variance-amplified model where birth and death transition rates are completely decoupled. The Monte Carlo simulations using Euler–Maruyama methodology demonstrate that the traditional SDE models underestimate ecological variability despite the fact that both SDE models have identical mean deterministic long-run outcomes.

Keywords: Continuous-Time Markov Chain; Itô Stochastic Differential Equations; demographic stochasticity; multispecies harvesting; Euler–Maruyama method; bioeconomic modeling

1. Introduction

Traditional approaches to multispecies ecology and bioeconomic management have largely relied on deterministic frameworks based on systems of nonlinear ordinary differential equations (ODEs). Pioneering work by Clark [1] and Chaudhuri [2] established the foundations for bioeconomic modeling of fisheries, providing theoretical frameworks for maximum sustainable yield and maximum economic rent. These deterministic methods assume continuous, homogeneous populations in infinite environments and implicitly treat demographic processes such as births, deaths, and predation as continuous and deterministic [3,4].

However, biological populations are inherently stochastic at the individual level. The random nature of births, deaths, and ecological interactions generates demographic stochasticity that can significantly alter population dynamics, particularly in small or heavily exploited populations [5]. This stochasticity can push populations past critical thresholds, amplify extinction risk, or generate unexpected dynamical behaviors that deterministic models cannot capture [6–8]. The importance of demographic stochasticity is well documented in conservation biology, where small populations face heightened extinction risk precisely due to random fluctuations [9,10].

To address these limitations, stochastic differential equations (SDEs) derived from continuous-time Markov chains (CTMCs) have become increasingly prevalent in population biology [11–13]. The diffusion approximation [14] provides a systematic framework

Check for updates

Academic Editor: Juan Ramón Torregrosa Sánchez

Published: 13 November 2026

Copyright: © 2026 by the authors. Licensee MDPI, Basel, Switzerland. This article is an open access article distributed under the terms and conditions of the Creative Commons Attribution (CC BY) license.

for transitioning from discrete-state CTMC models to continuous-state SDE formulations, yielding models that preserve the demographic stochasticity inherent in birth–death processes. A common approach in the literature constructs diffusion matrices based on net transition variances, effectively aggregating birth and death processes [3,15].

Nevertheless, this aggregation may have unintended consequences. By combining birth and death rates into net rates, the inherent stochastic variability arising from the separation of these processes can be obscured. Recent work by De Silva and Jang [16] demonstrated that different birth–death decompositions corresponding to the same deterministic model can yield substantially different stochastic dynamics. This insight suggests that the structural formulation of stochasticity—specifically, whether birth and death processes are aggregated or decoupled—can significantly influence model predictions and risk assessments.

This study explores the mathematical and ecological implications of structural noise refinement in a harvested two-species competition/predation framework. We formulate two distinct Itô SDE systems: a conventional aggregated model where diffusion coefficients are constructed from net transition variances, and a variance-amplified decoupled model where birth and death processes are explicitly separated and the true demographic variance is recovered. The two formulations share identical deterministic drift terms but differ fundamentally in their diffusion structure, providing a controlled comparison of the impact of noise formulation on population dynamics.

We conduct extensive Monte Carlo simulations using the Euler–Maruyama method to examine trajectory dynamics, probability density functions, and variance profiles. Our analysis aims to quantify how noise structure influences bioeconomic risk assessment, with particular attention to the probability of populations reaching critically low levels under sustained harvesting pressure. The results contribute to the growing literature on stochastic population modeling and have practical implications for fisheries management and conservation planning.

The remainder of this paper is organized as follows. Section 2 presents the deterministic baseline model and the CTMC formulation. Section 3 provides the rigorous derivation of the two SDE formulations. Section 4 presents theoretical analysis including positivity, boundedness, and equilibrium stability. Section 5 describes the numerical methodology and presents results using MATLAB 2019a. Section 6 discusses the implications of our findings, and Section 7 concludes with recommendations for stochastic modeling in bioeconomic applications.

2. Model Formulation

2.1. Deterministic System Baseline

We consider a two-species fishery system where population densities $x(t)$ and $y(t)$ interact through competition or predation and are subject to constant harvesting effort E. Following the classical bioeconomic framework of Chaudhuri [2] and Clark [1], the deterministic dynamics are governed by the following system of ordinary differential equations:

$$\begin{aligned} \frac{dx}{dt} &= (r - q_1 E)x - \frac{r}{K}x^2 - \alpha xy \\ \frac{dy}{dt} &= (s - q_2 E)y - \frac{s}{L}y^2 - \beta xy \end{aligned} \tag{1}$$

where r and s represent intrinsic growth rates; K and L denote environmental carrying capacities; q_1 and q_2 are catchability coefficients; and α and β quantify interspecies interaction strengths. The system possesses a non-trivial interior equilibrium (x^*, y^*) determined by solving the algebraic system $\frac{dx}{dt} = 0$ and $\frac{dy}{dt} = 0$.

https://doi.org/10.3390/cmsf2026015022

2.2. Continuous-Time Markov Chain (CTMC) Formulation

To incorporate demographic stochasticity, we transition from deterministic ODEs to a stochastic process. Let $\boldsymbol{X_1(t)}$ and $\boldsymbol{X_2(t)}$ denote the discrete random variables representing the population counts (not densities) of the two species in a spatial region of volume $\boldsymbol{V}$. The state space is $\mathbb{Z}_+^2 = \{0, 1, 2, ...\}^2$, and the process $\left\{X(t) = (X_1(t), X_2(t))^T : t \geq 0\right\}$ is a continuous-time Markov chain.

For a sufficiently small time interval $\Delta t > 0$, at most one birth or death event can occur. The possible changes $\Delta X = (\Delta X_1, \Delta X_2)^T$ and their corresponding probabilities are presented in Table 1.

Table 1. Possible state transitions for the CTMC model of the two-species harvesting system.

Event	Transition ΔX	Transition Probability
Birth of X_1	$(1, 0)^T$	$a_{11}X_1\Delta t$
Death/Harvest of X_1	$(-1, 0)^T$	$(b_{11}X_1 + \frac{r}{K}\frac{X_1^2}{V} + \alpha X_1X_2 + q_1EX_1)\Delta t$
Birth of X_2	$(0, 1)^T$	$a_{22}X_2\Delta t$
Death/Harvest of X_2	$(0, -1)^T$	$(b_{22}X_2 + \frac{s}{L}\frac{X_2^2}{V} + \beta X_1X_2 + q_2EX_2)\Delta t$
No change	$(0, 0)^T$	$1 - \Sigma_{i=1}^4 p_i$

Here, the parameters a_{11}, b_{11}, a_{22}, b_{22} satisfy $a_{11} - b_{11} = r$ and $a_{22} - b_{22} = s$. which ensures that the deterministic drift matches the ODE system (1). The terms $\frac{r}{K}\frac{X_1^2}{V}$ and $\frac{s}{L}\frac{X_2^2}{V}$ represent density-dependent mortality due to intraspecific competition, with V denoting the spatial volume that connects discrete population counts to continuous densities. The terms αX_1X_2 and βX_1X_2 represent interspecific interaction mortality.

Remark: The transition probabilities in Table 1 are expressed in terms of discrete population counts $X_1, X_2 \in \mathbb{Z}_+$, consistent with CTMC theory [17].

The transition rates are defined as:

$$b_1(X_1, X_2) = a_{11}X_1 \quad \text{(birth rate of species 1)}$$
$$d_1(X_1, X_2) = b_{11}X_1 + \frac{r}{K}\frac{X_1^2}{V} + \alpha X_1X_2 + q_1EX_1 \quad \text{(death/harvest rate of species 1)}$$
$$b_2(X_1, X_2) = a_{22}X_2 \quad \text{(birth rate of species 2)}$$
$$d_2(X_1, X_2) = b_{22}X_2 + \frac{s}{L}\frac{X_2^2}{V} + \beta X_1X_2 + q_2EX_2 \quad \text{(death/harvest rate of species 2)}$$

2.3. Diffusion Approximation to Itô SDE

Let $Y(t) = (Y_1(t), Y_2(t))^T = \left(\frac{X_1(t)}{V}, \frac{X_2(t)}{V}\right)^T$ denote the population densities. For large population sizes assuming system volume $V = 1$ without loss of generality, the CTMC can be approximated by a diffusion process [14]. The drift vector $\mu(Y)$ and diffusion matrix $\Sigma(Y)$ are derived from the infinitesimal mean and covariance:

Drift Vector

$$\mu(Y) = \begin{pmatrix} \mu_1(Y) \\ \mu_2(Y) \end{pmatrix} = \begin{pmatrix} (r - q_1E)y_1 - \frac{r}{K}y_1^2 - \alpha y_1y_2 \\ (s - q_2E)y_2 - \frac{s}{L}y_2^2 - \beta y_1y_2 \end{pmatrix}$$

Diffusion Matrix:

$$\Sigma(Y) = \begin{pmatrix} b_1 + d_1 & 0 \\ 0 & b_2 + d_2 \end{pmatrix}$$

where

$$b_1 + d_1 = a_{11}y_1 + b_{11}y_1 + \frac{r}{K}y_1^2 + \alpha y_1y_2 + q_1Ey_1$$

$$b_2 + d_2 = a_{22}y_2 + b_{22}y_2 + \frac{s}{L}y_2^2 + \boldsymbol{\beta} y_1 y_2 + q_2 E y_2$$

The resulting Itô SDE has the general form:

$$d\boldsymbol{Y}(t) = \boldsymbol{\mu}(\boldsymbol{Y}(t))dt + \boldsymbol{G}(\boldsymbol{Y}(t))d\boldsymbol{W}(t)$$

where $\boldsymbol{W}(t) = (\boldsymbol{W_1}(t), \boldsymbol{W_2}(t))^T$ is a two-dimensional standard Wiener process and $\boldsymbol{G}(\boldsymbol{Y})$ satisfies $\boldsymbol{G}(\boldsymbol{Y})\boldsymbol{G}(\boldsymbol{Y})^T = \boldsymbol{\Sigma}(\boldsymbol{Y})$ [18].

3. SDE Model Formulation

3.1. Standard Aggregate SDE Model

In the standard approach, diffusion coefficients are constructed from net transition variances. The diffusion matrix is given by:

$$\boldsymbol{G_{standard}} = \begin{pmatrix} \sqrt{(r + q_1 E + \frac{r}{K} y_1 + \boldsymbol{\alpha} y_2) y_1} & 0 \\ 0 & \sqrt{(s + q_2 E + \frac{s}{L} y_2 + \boldsymbol{\beta} y_1) y_2} \end{pmatrix}$$

The SDE system is:

$$\begin{aligned} d\boldsymbol{Y_1} &= \left[(r - q_1 E)y_1 - \tfrac{r}{K}y_1^2 - \boldsymbol{\alpha} y_1 y_2\right]dt + \sqrt{(r + q_1 E + \tfrac{r}{K}y_1 + \boldsymbol{\alpha} y_2)y_1}\, d\boldsymbol{W_1} \\ d\boldsymbol{Y_2} &= \left[(s - q_2 E)y_2 - \tfrac{s}{L}y_2^2 - \boldsymbol{\beta} y_1 y_2\right]dt + \sqrt{(s + q_2 E + \tfrac{s}{L}y_2 + \boldsymbol{\beta} y_1)y_2}\, d\boldsymbol{W_2} \end{aligned} \quad (2)$$

3.2. Variance-Amplified Decoupled SDE Model

When birth and death rates are explicitly separated rather than combined into net rates, the true demographic variance is recovered [19]. Using the decomposition:

$$\boldsymbol{a_{11} - b_{11} = r,\ a_{22} - b_{22} = s}$$

the diffusion matrix becomes:

$$\boldsymbol{G_{amplified}} = \begin{pmatrix} \sqrt{(a_{11} + b_{11})y_1 + q_1 E y_1 + \frac{r}{K} y_1^2 + \boldsymbol{\alpha} y_1 y_2} & \boldsymbol{0} \\ \boldsymbol{0} & \sqrt{(a_{22} + b_{22})y_2 + q_2 E y_2 + \frac{s}{L} y_2^2 + \boldsymbol{\beta} y_1 y_2} \end{pmatrix}$$

The SDE system is:

$$\begin{aligned} d\boldsymbol{Y_1} &= \left[(r - q_1 E)y_1 - \tfrac{r}{K} y_1^2 - \boldsymbol{\alpha} y_1 y_2\right]dt + \sqrt{(a_{11} + b_{11})y_1 + q_1 E y_1 + \tfrac{r}{K} y_1^2 + \boldsymbol{\alpha} y_1 y_2}\ d\boldsymbol{W_1} \\ d\boldsymbol{Y_2} &= \left[(s - q_2 E)y_2 - \tfrac{s}{L}y_2^2 - \boldsymbol{\beta} y_1 y_2\right]dt + \sqrt{(a_{22} + b_{22})y_2 + q_2 E y_2 + \tfrac{s}{L}y_2^2 + \boldsymbol{\beta} y_1 y_2}\, d\boldsymbol{W_2} \end{aligned} \quad (3)$$

Key Observation: Since $\boldsymbol{a_{ii} + b_{ii} > a_{ii} - b_{ii} = r_i}$ (for $\boldsymbol{i = 1, 2}$), the diffusion coefficients in the amplified model are strictly larger than those in the standard model when $\boldsymbol{a_{ii}}$ and $\boldsymbol{b_{ii}}$ are positive.

Specifically:

$$\boldsymbol{(a_{11} + b_{11}) > r,\ \ (a_{22} + b_{22}) > s}$$

Therefore, the variance-amplified model incorporates a strictly larger diffusion coefficient matrix while maintaining an identical drift vector $\boldsymbol{\mu}(\boldsymbol{Y})$.

4. Theoretical Analysis

4.1. Positivity of Solutions

A fundamental biological requirement is that population densities remain nonnegative. For the deterministic system (1), the positive quadrant $\mathbb{R}^2_+$ is invariant.

Theorem 1 (Positivity)**.** *For any nonnegative initial condition* $(x(0), y(0)) \in \mathbb{R}^2_+$ *, the solution of (1) remains nonnegative for all* $t \geq 0$.

Proof. Consider the boundary. If $x(t) = 0$, then $dx/dt = 0$, so $x(t)$ cannot become negative. Similarly, if $y(t) = 0$, then $dy/dt = 0$. Thus the boundary is invariant and the solutions remain in $\mathbb{R}^2_+$ [15,20]. □

For the SDE models (2) and (3), positivity is not guaranteed in the same strict sense due to the Brownian noise. However, for sufficiently large population sizes, the probability of reaching zero in finite time is negligible, and the SDE solutions remain positive with probability one under appropriate conditions [20,21].

4.2. Boundedness

Theorem 2 (Boundedness)**.** *The solutions of the deterministic system (1) are uniformly bounded for* $t \geq 0$.

Proof. From (1), if $x(t) > K$, then $dx/dt < 0$ (assuming $r - q_1 E > 0$). Therefore $x(t) \leq max\{x(0),K\}$. Similarly, $y(t) \leq max\{y(0),L\}$. Thus the solutions are bounded. □

4.3. Equilibria and Local Stability

The deterministic system has several equilibrium points:

1. Trivial equilibrium: $E_0 = (0,0)$
2. Boundary equilibria: $E_1 = \left(K\left(1 - \frac{q_1 E}{r}\right), 0\right) (if\ q_1 E < r)$,

$$E_2 = (0, L(1 - \frac{q_2 E}{s})) \ (if\ q_2 E < s)$$

3. Interior equilibrium: $E^* = (x^*, y^*)$

The interior equilibrium $E^* = (x^*, y^*)$ satisfies

$$\begin{array}{c} (r - q_1\, E) - \frac{r}{K}\, x^* - \alpha y^* = 0 \\ (s - q_2 E) - \frac{s}{L} y^* - \beta x^* = 0 \end{array} \tag{4}$$

The Jacobian matrix of system (1) is:

$$J(x,y) = \begin{pmatrix} r - q_1 E - \frac{2r}{K}x - \alpha y & -\alpha x \\ -\beta y & s - q_2 E - \frac{2s}{L} y - \beta x \end{pmatrix}$$

Local Stability of Interior Equilibrium: Using (4), we can simplify:

$$J_{11} = -\frac{r}{K} x^*, \ \ J_{22} = -\frac{s}{L} y^*$$

Then, at E^*, the trace and determinant of the Jacobian $J(x^*, y^*)$

$$tr(J) = -\frac{r}{K}\, x^* - \frac{s}{L}\, y^* < 0$$

$$det(J) = \frac{rs}{KL} x^* y^* - \alpha\beta x^* y^* = x^* y^* \left(\frac{rs}{KL} - \alpha\beta\right)$$

The interior equilibrium is locally asymptotically stable if:

$$\frac{rs}{KL} > \alpha\beta$$

which corresponds to the condition that intraspecific competition dominates interspecific competition at the equilibrium.

4.4. Stochastic Stability

For the SDE models, we consider stability in the sense of stochastic persistence [22]. The moment equations derived from (2) or (3) can be used to examine the evolution of the mean and variance. For the standard SDE model (2):

$$\frac{dE[Y_1]}{dt} = E[(r - q_1E)Y_1 - \frac{r}{K}Y_1^2 - \alpha Y_1Y_2]$$

$$\frac{dE[Y_2]}{dt} = E[(s - q_2E)Y_2 - \frac{s}{L}Y_2^2 - \beta Y_1Y_2]$$

These moment equations cannot be solved exactly due to the closure problem (higher-order moments appear). However, when fluctuations are small (large population sizes), the mean dynamics approximate the deterministic system (1) [3].

For the variance-amplified SDE model, the moment equations have the same drift structure but different diffusion coefficients, leading to identical mean dynamics but larger variance dynamics.

5. Numerical Simulation

Since obtaining accurate estimates of these parameters in field studies is problematic, the simulations can only be seen as qualitative instead of quantitative ones, as they show what regimes the model is capable of generating. The SDE systems (2) and (3) were solved numerically using the Euler–Maruyama method [23] with a time horizon of $\boldsymbol{T} = 10$, a time step of $\boldsymbol{\Delta t} = 0.001$ to ensure numerical stability, and 10,000 Monte Carlo trajectories, with initial conditions $\boldsymbol{y_1(0)} = 120$ and $\boldsymbol{y_2(0)} = 80$. The parameter values used were $\boldsymbol{r} = 1.0$, $\boldsymbol{s} = 0.8$, $\boldsymbol{K} = 200$, $\boldsymbol{L} = 150$, $\boldsymbol{\alpha} = 0.002$, $\boldsymbol{\beta} = 0.0015$, $\boldsymbol{q_1} = 0.01$, $\boldsymbol{q_2} = 0.01$, and $\boldsymbol{E} = 20$ for constant harvesting effort based on the literature. For the variance-amplified SDE model, we employed $\boldsymbol{a_{11}} = 2.0$, $\boldsymbol{b_{11}} = 1.0$, $\boldsymbol{a_{22}} = 1.6$, and $\boldsymbol{b_{22}} = 0.8$, which satisfy $\boldsymbol{a_{11} - b_{11} = 1.0 = r}$ and $\boldsymbol{a_{22} - b_{22} = 0.8 = s}$. MATLAB 2019a was used for the data validation and visualization.

Figure 1 presents representative sample paths for species x and y for both SDE models, plotted alongside the deterministic ODE solution. The standard SDE model's sample paths closely track the deterministic trajectory, exhibiting relatively modest fluctuations around the equilibrium. In striking contrast, the variance-amplified SDE model displays substantially wider oscillations with frequent path crossings and considerably larger deviations from the deterministic solution. This qualitative difference arises directly from the structural separation of birth and death rates, as the standard model implicitly aggregates these processes, reducing the effective stochastic variability, while the amplified model explicitly retains the individual contributions of birth and death processes, thereby recovering the full demographic variance that is obscured in conventional formulations.

In order to evaluate long-term stability and stochastic fluctuations under continuous harvesting, statistics such as (μ, σ, and CV) calculated at $t = 10$ from 10,000 different Monte Carlo runs are presented in Table 2, for both the standard and variance-amplified equations.

Several key findings emerge from these results. First, both SDE models produce nearly identical mean values, confirming that both formulations correctly preserve the deterministic drift. Second, the variance-amplified model exhibits substantially larger standard deviations, with species X showing a 37% increase and species Y showing a 38% increase over the standard model. Third, the coefficients of variation are consistently higher in the amplified model, with increases ranging from 37% to 40%, representing substantial amplification of relative variability that cannot be captured by the aggregate formulation.

https://doi.org/10.3390/cmsf2026015022

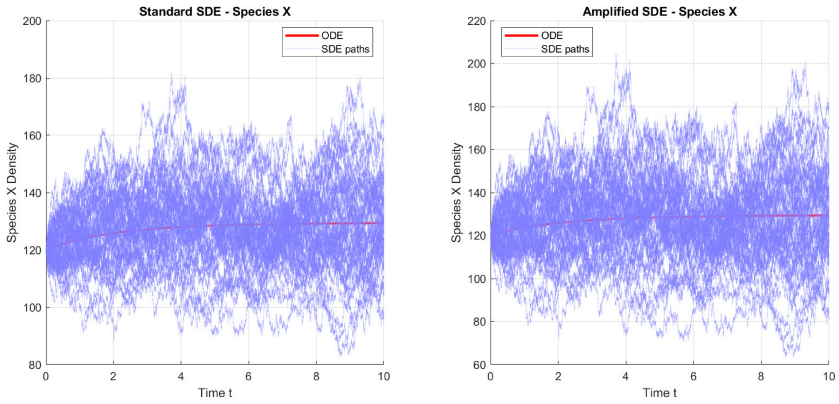
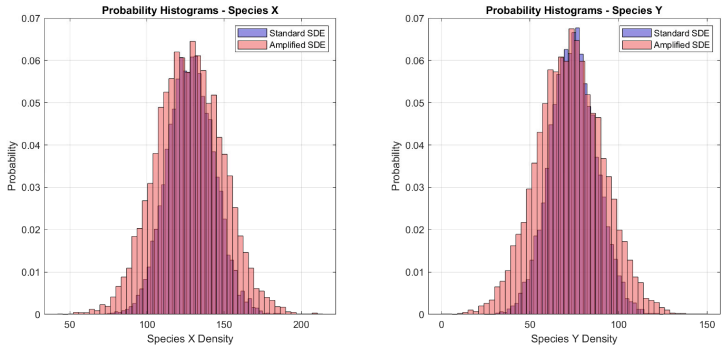


Figure 1. Representative sample path trajectories for the two-species fishery model. Left panels: Standard SDE model. Right panels: Variance-amplified SDE model. Red lines denote the deterministic ODE solution; blue lines show 50 randomly selected stochastic trajectories.

Table 2. Comparative statistical performance at $t = 10$ across 10,000 Monte Carlo path trajectories.

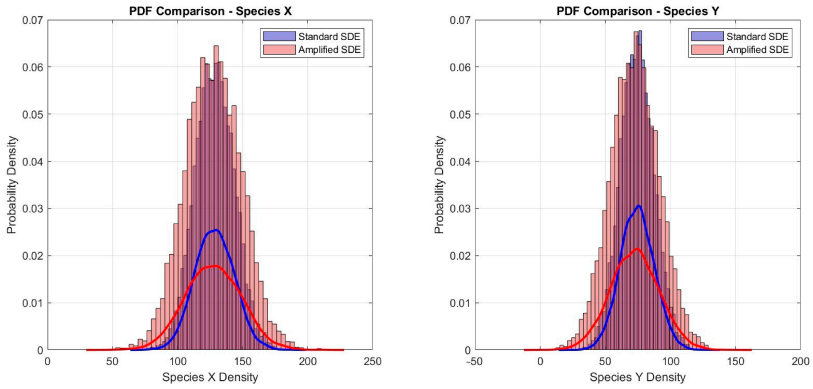
System Model	Variable	Mean (μ)	Standard Deviation (σ)	Coefficient of Variation (CV)
Standard SDE Model	Species X	124.8027	16.0139	0.1283
	Species Y	84.6853	13.7462	0.1623
Amplified SDE Model	Species X	124.3939	21.9643	0.1766
	Species Y	83.3543	18.9238	0.2270

Figures 2 and 3 display empirical probability histograms and kernel density estimates for both species at $t = 10$. The variance-amplified SDE model produces flatter, wider distributions compared to the sharper distributions of the standard SDE model, indicating increased probability mass in the tails, particularly at low population densities. This translates to heightened extinction risk and greater vulnerability to population crashes under sustained harvesting pressure, as while the mean dynamics remain identical, the probability of population dips into critically low levels is substantially higher in the amplified model.



(**a**) (**b**)

Figure 2. Empirical probability histograms for (**a**) species X and (**b**) species Y at t = 10 from 10,000 Monte Carlo trajectories. Blue bars represent the standard SDE model; red bars represent the variance-amplified SDE model.



(**a**) (**b**)

Figure 3. Kernel density estimates comparing probability distributions for (**a**) species X and (**b**) species Y at $t = 10$. Blue lines denote standard SDE model; red lines denote variance-amplified SDE model.

Figure 4 illustrates the sensitivity of the coefficient of variation to changes in harvesting effort E across the range 10 to 30. For both species, increasing E leads to higher CV values in both models, indicating that harvesting amplifies population variability. However, the amplified model consistently shows higher CV values across all harvesting effort levels, and the gap between the two models widens at higher E values, suggesting that the structural underestimation of variance by standard aggregate models becomes more pronounced under intensive harvesting regimes, precisely where accurate risk assessment is most critical for conservation and management purposes.

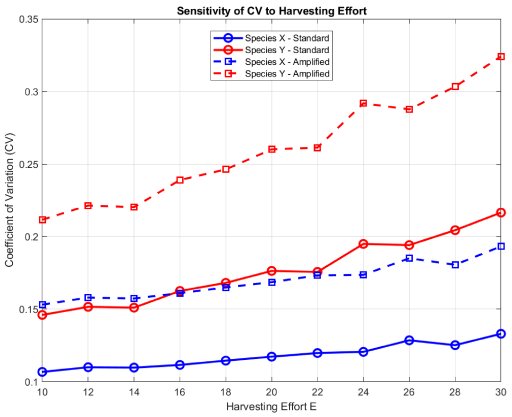


Figure 4. Coefficient of variation as a function of harvesting effort E. Solid lines indicate standard SDE model; dashed lines indicate variance-amplified SDE model. Blue lines denote species X; red lines denote species Y.

6. Discussion

The results of this study demonstrate a fundamental mathematical insight: standard aggregation of birth and death processes in SDE formulations systematically underestimates stochastic variability. This underestimation arises because the diffusion coefficient in the standard model implicitly assumes that the variance of the net change is equal to the sum of the variances of births and deaths, whereas when births and deaths are separated, the total variance is larger because the individual contributions are not canceled by aggregation. Specifically, for species 1, the inequality,

$$(a_{11} + b_{11})y_1 + q_1 E y_1 + (r/K)y_1^2 + \alpha y_1 y_2 > (r + q_1 E)y_1 + (r/K)y_1^2 + \alpha y_1 y_2$$

holds since $a_{11} + b_{11} > a_{11} - b_{11} = r$, meaning the variance-amplified model produces strictly larger diffusion coefficients for any positive a_{11} and b_{11}. This mathematical property has important consequences for risk assessment, as the amplified model's wider probability distributions indicate that populations are more likely to experience extreme fluctuations, including near-extinction events [24,25], suggesting that conservation and management decisions based on standard aggregate models may be dangerously optimistic about population resilience.

From an ecological perspective, the amplification of variance reflects the demographic stochasticity inherent in biological populations, where birth and death are fundamentally separate random processes whose decoupling in the variance-amplified model more accurately captures true demographic variability. The aggregated model, while mathematically simpler, effectively smooths over this variability by assuming that birth and death rates can be combined into a single net rate without loss of information. This distinction is particularly important for exploited populations, as harvesting introduces additional mortality that increases stochastic variance through the $q_i E y_i$ terms in the diffusion coefficients, and the amplified model more transparently demonstrates how harvesting contributes to demographic variance. Our findings are consistent with previous work by Allen, who noted that different stochastic formulations corresponding to the same deterministic model can yield different statistical properties, and by De Silva and Jang, who demonstrated that alternative birth–death decompositions in a phytoplankton-zooplankton model produced different stochastic dynamics, thus extending these results to a harvested two-species fishery model with explicit comparison of standard and amplified formulations.

Several limitations of this study should be acknowledged. We assumed constant harvesting effort and constant parameters, whereas in reality harvesting strategies may be adaptive and environmental conditions may vary, suggesting that future work could incorporate seasonal harvesting or stochastic environmental forcing. The analysis was restricted to two species, and extensions to multispecies food webs would be valuable to assess whether the variance amplification effect persists or becomes more pronounced in complex communities. We also did not consider spatial structure, though spatial heterogeneity can affect population dynamics and may interact with demographic stochasticity in non-trivial ways. Additionally, the model parameters were chosen for illustrative purposes, and applying the model to specific fisheries systems would require parameter estimation from empirical data, which remains an important direction for future research.

7. Conclusions

This study has systematically compared two Itô SDE formulations for a harvested two-species fishery model: a standard aggregate-diffusion model and a variance-amplified model with explicit birth–death decoupling. Through rigorous CTMC-to-SDE derivation and extensive Monte Carlo simulations, we have demonstrated that structural noise refinement matters significantly, as while both SDE models preserve the same deterministic mean dynamics, they differ substantially in their diffusion structure. Furthermore, standard models underreport variability, as the aggregate SDE model systematically underestimates population variance, producing narrower probability distributions and lower coefficients of variation. In contrast, amplified models reveal hidden risk, as the variance-amplified formulation reveals significantly wider population fluctuations and increased extinction risk, particularly under high harvesting pressure. These findings carry important conservation implications, as management decisions based on standard aggregate stochastic models may dangerously overestimate population resilience and underestimate extinction vulnerability. The practical implications of these findings are clear: in bioeconomic modeling and fisheries management, the choice of stochastic formulation is not merely a technical detail but a

substantive modeling decision that can significantly affect risk assessment. We therefore recommend that stochastic bioeconomic models explicitly separate birth and death rates rather than aggregating them into net rates, especially when evaluating population viability under harvesting regimes. Future research should extend these findings to incorporate environmental stochasticity, adaptive harvesting strategies, and spatial structure, as the variance-amplified framework provides a more realistic foundation for these extensions and for the development of robust management strategies in the face of demographic uncertainty.

Author Contributions: Conceptualization, P.T.T., and M.M.D.S.; methodology, P.T.T., and M.M.D.S.; formal analysis, P.T.T.; software, P.T.T.; writing—original draft preparation, P.T.T.; writing—review and editing, M.M.D.S.; supervision, M.M.D.S. All authors have read and agreed to the published version of the manuscript.

Funding: This research received no external funding.

Institutional Review Board Statement: Not applicable.

Informed Consent Statement: Not applicable.

Data Availability Statement: The data/codes supporting reported results are available from the corresponding author upon request.

Conflicts of Interest: The authors declare no conflict of interest.

References

1. Clark, C.W. *Mathematical Bioeconomics: The Mathematics of Conservation*, 3rd ed.; John Wiley & Sons: Hoboken, NJ, USA, 2010.
2. Chaudhuri, K. A bioeconomic model of harvesting a multispecies fishery. *Ecol. Model.* **1986**, *32*, 267–279. [CrossRef]
3. Allen, E.J. *Modeling with Ito Stochastic Differential Equations*; Springer: Dordrecht, The Netherlands, 2007.
4. Boglou, K.; Akritas, A.; Koulakiotis, D.; Papavassiliou, E. Numerical methods for stochastic differential equations. *AIP Conf. Proc.* **2018**, *1978*, 470003.
5. Lande, R.; Engen, S.; Saether, B.E. *Stochastic Population Dynamics in Ecology and Conservation*; Oxford University Press: Oxford, UK, 2003.
6. Dennis, B. Allee effects in stochastic populations. *Oikos* **2002**, *96*, 389–401. [CrossRef]
7. Allen, E.J.; Allen, L.J.S.; Arciniega, A.; Greenwood, P.E. Construction of equivalent stochastic differential equation models. *Stoch. Anal. Appl.* **2008**, *26*, 274–297. [CrossRef]
8. Henderson, D.; Plaschko, P. *Stochastic Differential Equations in Science and Engineering*; World Scientific: Singapore, 2006.
9. Melbourne, B.A.; Hastings, A. Extinction risk depends strongly on factors contributing to stochasticity. *Nature* **2008**, *454*, 100–103. [CrossRef] [PubMed]
10. Ovaskainen, O.; Meerson, B. Stochastic models of population extinction. *Trends Ecol. Evol.* **2010**, *25*, 643–652. [CrossRef] [PubMed]
11. Krstic, M.; Jovanovic, M. On stochastic population model with the Allee effect. *Math. Comput. Model.* **2010**, *52*, 370–379. [CrossRef]
12. Jovanovic, M.; Krstic, M. The influence of time-dependent delay on behavior of stochastic population model with the Allee effect. *Appl. Math. Model.* **2015**, *39*, 733–746. [CrossRef]
13. Jovanovic, M.; Krstic, M. Extinction in stochastic predator-prey population model with Allee effect on prey. *Discrete Contin. Dyn. Syst. B* **2017**, *22*, 2651. [CrossRef]
14. Gardiner, C.W. *Stochastic Methods: A Handbook for the Natural and Social Sciences*, 4th ed.; Springer: Berlin, Germany, 2009.
15. Mao, X. *Stochastic Differential Equations and Applications*, 2nd ed.; Woodhead Publishing: Cambridge, UK, 2007.
16. De Silva, T.M.M.; Jang, S.R.-J. Stochastic modeling of phytoplankton-zooplankton interactions with toxin producing phytoplankton. *J. Biol. Syst.* **2018**, *26*, 87–106. [CrossRef]
17. Allen, L.J.S. *An Introduction to Stochastic Processes with Applications to Biology*, 2nd ed.; CRC Press: Boca Raton, FL, USA, 2011.
18. Brauer, F.; Soudack, A.C. On constant effort harvesting and stocking in a class of predator-prey systems. *J. Theor. Biol.* **1982**, *95*, 247–252. [CrossRef]
19. Aguirre, P.; Gonzalez-Olivares, E.; Torres, S. Stochastic predator-prey model with Allee effect on prey. *Nonlinear Anal. Real World Appl.* **2013**, *14*, 768–779. [CrossRef]
20. Higham, D.J. An algorithmic introduction to numerical simulation of stochastic differential equations. *SIAM Rev.* **2001**, *43*, 525–546. [CrossRef]

21. Kloeden, P.E.; Platen, E. *Numerical Solution of Stochastic Differential Equations*; Springer: Berlin, Germany, 1992.
22. Tran, K.; Yin, G. Stochastic competitive Lotka-Volterra ecosystems under partial observation: Feedback controls for permanence and extinction. *J. Frankl. Inst.* **2014**, *351*, 4039–4064. [CrossRef]
23. Zhang, B.; Wang, H.; Lv, G. Exponential extinction of a stochastic predator-prey model with Allee effect. *Phys. A* **2018**, *507*, 192–204. [CrossRef]
24. Wang, G.; Liang, X.G.; Wang, F.Z. The competitive dynamics of populations subject to an Allee effect. *Ecol. Model.* **1999**, *124*, 183–192. [CrossRef]
25. Zhou, S.R.; Liu, Y.F.; Wang, G. The stability of predator-prey systems subject to the Allee effects. *Theor. Popul. Biol.* **2005**, *67*, 23–31. [CrossRef] [PubMed]

Disclaimer/Publisher's Note: The statements, opinions and data contained in all publications are solely those of the individual author(s) and contributor(s) and not of MDPI and/or the editor(s). MDPI and/or the editor(s) disclaim responsibility for any injury to people or property resulting from any ideas, methods, instructions or products referred to in the content.